Microsc. Microanal. 18, 705–710, 2012
doi:10.1017/S1431927612001304

Microscopy AND Microanalysis

Ad Hoc Auto-Tuning of Aberrations Using High-Resolution STEM Images by Autocorrelation Function

Hidetaka Sawada,[1,*] Masashi Watanabe,[2] and Izuru Chiyo[1]

[1]*JEOL Ltd., EMBU, 3-1-2 Musashino, Akishima, Tokyo 196-8558, Japan*
[2]*Department of Materials Science and Engineering, Lehigh University, Bethlehem, PA 18015, USA*

Abstract: A method for measurement of the aberration status from high-resolution dark-field images is developed using scanning transmission electron microscopy (STEM), called the Segmented Image Autocorrelation function Matrix (SIAM). The method employs an autocorrelation function from the segmented area in the defocused STEM images from an aligned crystalline specimen to measure the defocus and twofold astigmatism for the probe-forming system. The values measured using this method can be fed directly back to the instrument by changing the strength of the stigmator and the objective lens of the microscope. It is successfully demonstrated that the feedback system can automatically correct the defocus and twofold astigmatism of the microscope after several iterations using practical STEM images from an actual crystalline specimen.

Key words: high-resolution STEM image, autocorrelation function, aberration, auto-tuning, crystalline specimen

Introduction

Spherical aberration correctors (Rose, 1990; Haider et al., 1998; Krivanek et al., 1999; Hosokawa et al., 2006; Sawada et al., 2009) for probe-forming systems have been widely used in high-resolution structural and chemical analytical studies with scanning transmission electron microscopy (STEM). Recent practical aberration correctors have the capability to compensate for up to fourth-order residual aberrations as well as third-order spherical aberrations. Parasitic aberrations such as twofold astigmatism, axial coma, threefold astigmatism, star aberration, fourfold astigmatism, etc. can be adjusted by using the optical elements of the microscope and the corrector. For the automatic correction of these aberrations using software, aberration measurements in the probe-forming lens system are essential. Several methods for the aberration measurement have been reported, for example, using a standard amorphous-film specimen with nanometallic particles (Haider et al., 2000), Ronchigrams (Cowley, 1986; Dellby et al., 2001; Ramasse & Bleloch, 2005; Yamazaki et al., 2006; Sawada et al., 2008; Lupini et al., 2010), or medium-resolution high-angle annular dark-field (HAADF) images (Rudnaya et al., 2011). Sawada et al. (2008) developed an aberration measurement procedure that uses the autocorrelation function from a Ronchigram, called the Segmented Ronchigram Autocorrelation function Matrix (SRAM) method. In this method, the autocorrelation functions obtained from segmented areas of the Ronchigram are utilized to obtain the values of the second-order differential of the wave aberration for each aberration. After the collection of these auto-correlation functions from each angular area segmented in the Ronchigram, the aberrations of the probe-forming system can be calculated.

The auto-tuning systems using these aberration measurement methods have been established and utilized routinely, with a standard specimen. However, for observation of atomic-resolution images in actual crystalline specimens, *ad hoc* manual adjustment of the defocus and twofold astigmatism is generally required immediately before a high-resolution image is recorded. There are two primary reasons required for the manual fine-tuning. First, any fine instability of the instrument and corrector may cause a small drift of the aberration status when the standard specimen for aberration tuning is exchanged for the actual crystalline specimen. Small drifts in higher order aberrations such as star aberration and fourfold astigmatism would not influence the system aberration very much. In contrast, any small drift of first-order aberrations (defocus and twofold astigmatism) can significantly change the system aberration. Therefore, in general, these first-order aberrations must be adjusted on the actual (crystalline) specimen. Furthermore, precision in the first-order aberration tuning achieved by an experienced operator is still superior to that through the software packages presently available for aberration tuning. If aberrations were measurable directly from actual atomic-resolution STEM images of a real crystalline specimen instead of the standard specimen, *ad hoc* aberration auto-tuning could be applied instantaneously before the recording of the final images during structural image observation. Thus, an *ad hoc* aberration measurement method using high-resolution STEM images has been developed, which is called the Segmented Image Autocorrelation function Matrix (SIAM) method (Sawada et al., 2011). In

Received February 19, 2012; accepted April 30, 2012
*Corresponding author. E-mail: hidesawada@mail.goo.ne.jp

Table 1. First-Order Aberrations (Sawada et al., 2008).

Aberration: Notation	Coefficient	Wave Aberration	Geometrical Aberration
Defocus: O_2	o_2	$\mathrm{Re}\{\frac{1}{2} O_2 \omega\bar{\omega}\}$	$O_2\omega = o_2\alpha \exp(i\theta) = o_2\alpha(\cos\theta + i\cdot\sin\theta)$
Twofold astigmatism: A_2	$a_2 \exp(2i\theta_{a2})$	$\mathrm{Re}\{\frac{1}{2} A_2\bar{\omega}^2\}$	$A_2\bar{\omega} = a_2\alpha \exp i(2\theta_{a2} - \theta)$ $= a_2\alpha\{\cos(2\theta_{a2} - \theta) + i\cdot\sin(2\theta_{a2} - \theta)\}$

this approach, a series of autocorrelation functions from segmented areas of high-resolution STEM images of a crystalline specimen is utilized to calculate and tune the aberrations of the defocus and twofold astigmatism. In this article, the principles and experimental results of the SIAM method are reported.

Methods

Generalized Probe-Function Distribution with First-Order Geometrical Aberration

A HAADF-STEM image, where the intensity of the image caused by scattered electrons reveals the atomic column arrangement of the specimen, is used for this aberration measurement. Mathematical calculation of the autocorrelation F_{AC} $(= \Im^{-1}[|\Im[I]|^2])$ of an image I is used for the aberration measurements. In the SIAM method, the autocorrelation function from a HAADF-STEM image is supposed to be a probe shape function with residual aberrations if it can be assumed that the intensity map of each atomic column is isotropic. Here, the details of image processing and aberration measurement procedure for the SIAM method are summarized. Suppose that a HAADF-STEM image I can be described simply by a convolution of the specimen information S with a probe function P, i.e., $I = S \otimes P$, where $\otimes$ denotes a convolution operation. The autocorrelation function F_{AC} of $I = S \otimes P$ is $F_{AC} = \Im^{-1}[\Im[S \otimes P]^2] = \Im^{-1}[\Im[S]^2 \cdot \Im[P]^2]$, where $\Im$ and $\Im^{-1}$ are the Fourier and inverse Fourier transformations, respectively. The atomic potential is assumed to be a delta function as $\Im[\delta] = 1$ because the atomic potential should ideally be sharper rather than the defocused probe even if aberration correction is applied, then $F_{AC} = \Im^{-1}[\Im[P]^2] = |P|^2$. The probe function can be assumed to be the Gaussian function, $\exp(-(x^2 + y^2)/2d)$. Due to aberration, the probe shape can deviate from the ideal aberration-free round distribution and become oval shaped. Therefore, the probe function with aberration can be described by $\exp(-(Ax^2 + By^2 + 2Csy)/2d)$. Here, A, B, and C are the parameters to describe the oval distribution with certain aberrations. Thus, the autocorrelation function of a high-resolution image can be expressed as

$$F_{AC} \propto |P|^2 \propto \exp\left(-\frac{Ax^2 + By^2 + 2Cxy}{d}\right). \tag{1}$$

We can measure the focus and twofold astigmatism of the probe through image processing, where the contour of the autocorrelation function from an atomic-resolution dark-field image is fitted as an oval function of $Ax^2 + By^2 + 2Cxy$.

Measurement Procedure of First-Order Geometrical Aberrations from Probe-Function Distributions

The complex angle can be expressed as $\boldsymbol{\omega} = \alpha \exp(i\theta) = \omega_u + i\omega_v = \lambda(u + iv)$, where λ is the wavelength, has a convergence angle α and azimuth θ. $\bar{\boldsymbol{\omega}} = \alpha \exp(-i\theta)$ is the complex conjugate of $\boldsymbol{\omega}$. The first-order aberrations considered in this article are listed in Table 1.

The x and y components (X, Y) of the geometrical aberration at the specific angle α of the probe including the first-order aberrations can be written as

$$X = o_2 \cos\theta + a_2 \cos(2\theta_{a2} - \theta), \tag{2a}$$

$$Y = o_2 \sin\theta + a_2 \sin(2\theta_{a2} - \theta). \tag{2b}$$

Using $a_{2x} = \cos 2\theta_{a2}$ and $a_{2y} = \sin 2\theta_{a2}$,

$$\sin\theta = \frac{(o_2 + a_{2X})Y - a_{2Y}X}{o_2^2 - a_{2Y}^2 - a_{2X}^2}, \tag{3a}$$

$$\cos\theta = \frac{(o_2 - a_{2X})X - a_{2Y}Y}{o_2^2 - a_{2X}^2 - a_{2Y}^2}. \tag{3b}$$

Then we have the oval function at the specific angle, described by

$$\frac{\left(\begin{array}{l}(o_2^2 - 2o_2a_{2X} + a_{2X}^2 + a_{2Y}^2)X^2 \\ \quad + (o_2^2 + 2o_2a_{2X} + a_{2X}^2 + a_{YX}^2)Y^2 \\ \quad - 4o_2a_{2Y}XY\end{array}\right)}{(o_2^2 - a_{2Y}^2 - a_{2X}^2)^2} = 1. \tag{4}$$

Comparing $AX^2 + BY^2 + 2CXY = 1$ and equation (4), we obtain

$$A = \frac{(o_2^2 - 2o_2a_{2X} + a_{2X}^2 + a_{YX}^2)}{(o_2^2 - a_{2Y}^2 - a_{2X}^2)^2}, \tag{5a}$$

$$B = \frac{(o_2^2 + 2o_2a_{2X} + a_{2X}^2 + a_{2Y}^2)}{(o_2^2 - a_{2Y}^2 - a_{2X}^2)^2}, \tag{5b}$$

$$C = \frac{-2o_2a_{2Y}}{(o_2^2 - a_{2Y}^2 - a_{2X}^2)^2}. \tag{5c}$$

If a sufficiently large defocus o_2 is applied, the higher order terms of a_{2X} and a_{2Y} are negligible, and then

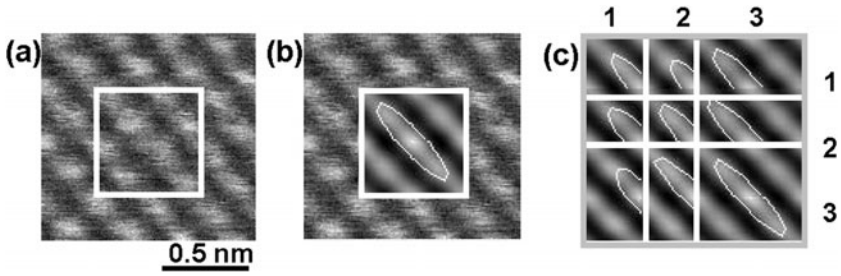

Figure 1. a: Defocused dark-field STEM image of [100]-projected $SrTiO_3$ with a size of 128 × 128 pixels, using a scan speed of 20 μs/pixel. **b:** The pattern of the autocorrelation function from 64 × 64 pixels in panel **a**, with the ellipse fitting shown by the white line. **c:** A 3 × 3 matrix of segmentations for autocorrelation patterns, where each pattern has an overlapped region.

$$A = \frac{(o_2 - 2a_{2X})}{o_2^3}, \tag{6a}$$

$$B = \frac{(o_2 + 2a_{2X})}{o_2^3}, \tag{6b}$$

$$C = \frac{-2a_{2Y}}{o_2^3}. \tag{6c}$$

Each aberration is calculated from the coefficients (A, B, C) of the oval function obtained from the contour of the autocorrelation function with a constant k, as given by

$$o_2 = k\sqrt{\frac{2}{A+B}}, \tag{7a}$$

$$a_{2X} = \frac{k\cdot(B-A)}{2(A+B)}\cdot\sqrt{\frac{2}{A+B}}, \tag{7b}$$

$$a_{2Y} = -\frac{k\cdot C}{A+B}\sqrt{\frac{2}{A+B}}, \tag{7c}$$

where $A + B > 0$. When we obtain two images by changing the defocus do_2, equation (2) becomes

$$X = (o_2 + do_2)\cos\theta + a_2\cos(2\theta_{a2} - \theta), \tag{8a}$$

$$Y = (o_2 + do_2)\sin\theta + a_2\sin(2\theta_{a2} - \theta). \tag{8b}$$

If the oval distributions of the probe functions determined from two images recorded at two different defocus conditions I and II are given as $A_I X^2 + B_I Y^2 + 2C_I XY = 1$ and $A_{II} X^2 + B_{II} Y^2 + 2C_{II} XY = 1$, the two defocus values can be expressed as $o_2 = k\sqrt{2/(A_I + B_I)}$ and $o_2 + do_2 = k\sqrt{2/(A_{II} + B_{II})}$. do_2 indicates the difference in defocus at two different defocus conditions. When the images at defocuses I and II are recorded under and over the defocused condition, the constant k is derived from do_2 in equation (9):

$$k = \frac{do_2}{\sqrt{\frac{2}{A_I + B_I}} + \sqrt{\frac{2}{A_{II} + B_{II}}}}. \tag{9}$$

The first-order geometrical aberrations of the defocus and twofold astigmatism are measurable using autocorrelation functions from more than two images by the oval shape fitting. When several HAADF-STEM images are taken at different defocus values with the same focal step (do_2), the defocus values at each step can be given by

$$o_{2I} = k\sqrt{\frac{2}{A_I + B_I}}, \tag{10a}$$

$$o_{2II} = o_{2I} + do_2 = k\sqrt{\frac{2}{A_{II} + B_{II}}}, \tag{10b}$$

$$o_{2III} = o_{2I} + 2do_2 = k\sqrt{\frac{2}{A_{III} + B_{III}}}, \tag{10c}$$

$$o_{2I}^2 = k^2\,\frac{2}{A_I + B_I}, \tag{11a}$$

$$o_{2II}^2 = k^2\,\frac{2}{A_{II} + B_{II}}, \tag{11b}$$

$$o_{2III}^2 = k^2\,\frac{2}{A_{III} + B_{III}}. \tag{11c}$$

The minimum o_2^2 value can be determined mathematically from obtained $o_{2i}^2 (i = I, II, III \ldots)$ values via fitting, which also provides the Gaussian defocus and constant k values. Then, each aberration can be calculated using equation (7).

Results

Determination of Probe-Function Distribution from a Defocused Image

The SIAM method was tested using 200- or 300-kV high-resolution STEM instruments, which were equipped with probe-forming aberration correctors. Prior to applying the SIAM method, residual aberrations up to the fourth-order aberration as well as the third-order spherical aberration were compensated using the existing auto-tuning systems (Haider et al., 2000; Sawada et al., 2008). For testing the SIAM method, a crystalline specimen of [100]-projected $SrTiO_3$ was used.

Figure 1b shows an autocorrelation function pattern from the selected central part of an HAADF-STEM image from [100]-projected $SrTiO_3$ (Fig. 1a). The elongated ellipse in the autocorrelation function pattern shown in Figure 1b

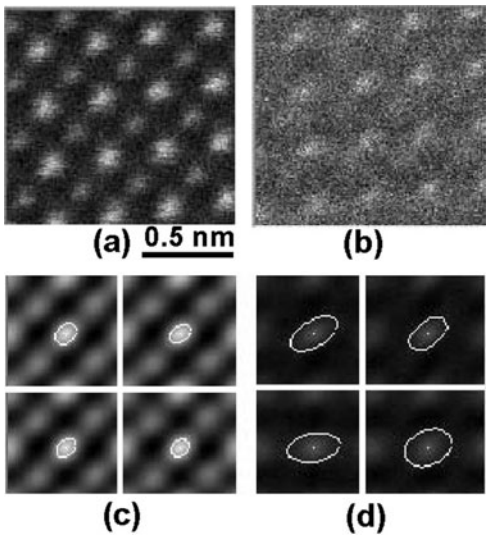

Figure 2. High-resolution HAADF-STEM images from the [100]-projected $SrTiO_3$ in the conditions that the defocus was intentionally applied: (**a**) underfocused and (**b**) overfocused images with defocus separation of 20 nm. Panels **c** and **d** are the patterns of the autocorrelation functions from panels **a** and **b** with the elliptical fittings indicated as white lines.

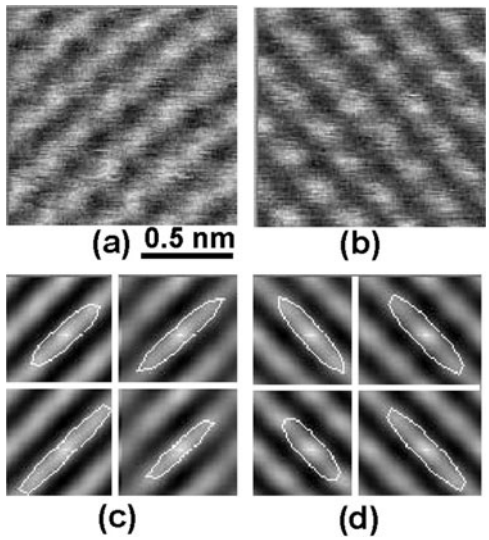

Figure 3. High-resolution HAADF-STEM images from the [100]-projected $SrTiO_3$ in the conditions that the twofold astigmatism was intentionally applied: (**a**) underfocused and (**b**) overfocused images with defocus separation of 20 nm. Panels **c** and **d** are the patterns of the autocorrelation functions from panels **a** and **b** with the elliptical fittings indicated as white lines.

indicates that the distribution of probe shape in the HAADF-STEM image is no longer symmetrically round and is influenced by some magnitude of twofold astigmatism. The autocorrelation function is calculated from a small-segmented area in the STEM image (not from a whole field of view) to reduce the periodicity of the crystalline lattice. Then, the values of the defocus and twofold astigmatism are measured from the central peak in the autocorrelation pattern by fitting to an elliptical shape (Fig. 1b). Multiple autocorrelation patterns from the image are used for determination of the aberration values to improve the statistics by averaging the individual minor variations arising from local differences in the specimen structure of each segmented area. Figure 1c shows multiple autocorrelation patterns where the image was divided into a 3×3 matrix of segmentations. These elliptical patterns are essentially the same unless the local structures of individual segmented images are influenced by the local structure.

Aberration Determination by the SIAM Method

Here, examples of aberration measurements by the SIAM method are shown. More than a pair of defocused STEM images are required to determine the absolute values of these aberrations, which are converted from the calibrated defocus values. Figures 2 and 3 show a pair of HAADF-STEM images obtained in underfocus and overfocus conditions from the crystalline $SrTiO_3$ specimen, with intentionally applied defocus and twofold astigmatism, respectively. In both the applications, defocus was changed from the initial defocus value to -10 nm and $+10$ nm in image acquisitions for the aberration measurement. The defocus step was calibrated beforehand by measuring the distance of a crystalline lattice on Ronchigram (Lin & Cowley, 1986). In addition to a pair of defocused images, four patterns of autocorrelation functions extracted from the corresponding defocused images are also shown in Figures 2 and 3.

In the example shown in Figure 2, the original focus position was intentionally deviated from the optimum focal point, and two defocused images were taken with the defocus difference of 20 nm. Although the atomic columns are imaged as rounder shapes in comparison with the prior case shown in Figure 1, the image qualities are significantly different between Figures 2a and 2b. Figure 2a is relatively sharper and shows higher contrast than Figure 2b. The larger elliptical patterns resulting from the autocorrelation function in Figure 2d indicate that the defocus is significantly deviated from the Gaussian focus, whereas the elliptical patterns in Figure 2c are much smaller. From these elliptical patterns of the autocorrelation functions, the first-order aberrations were determined. The original defocus and twofold astigmatism values that were determined were 5.52 nm and 1.51 nm, respectively. For the twofold astigmatism, not only the actual value but also the angle of the stigmated direction can be determined. In this case, the angle was 79.50°.

Results of another example with the intentional addition of twofold astigmatism are shown in Figure 3. Similar to the previous example, the (a) underfocused and (b) overfocused images taken with a 20-nm focus separation are shown with the extracted elliptical patterns of the autocorrelation functions (c, d). Fitting results shown with white lines based on the intensity contour in the autocorrelation function patterns in Figures 3c and 3d result in rather elongated oval shapes because of the residual twofold astigmatism. Furthermore, the elliptical patterns of the autocorrelation in Figure 3c are rotated by 90° compared to those in

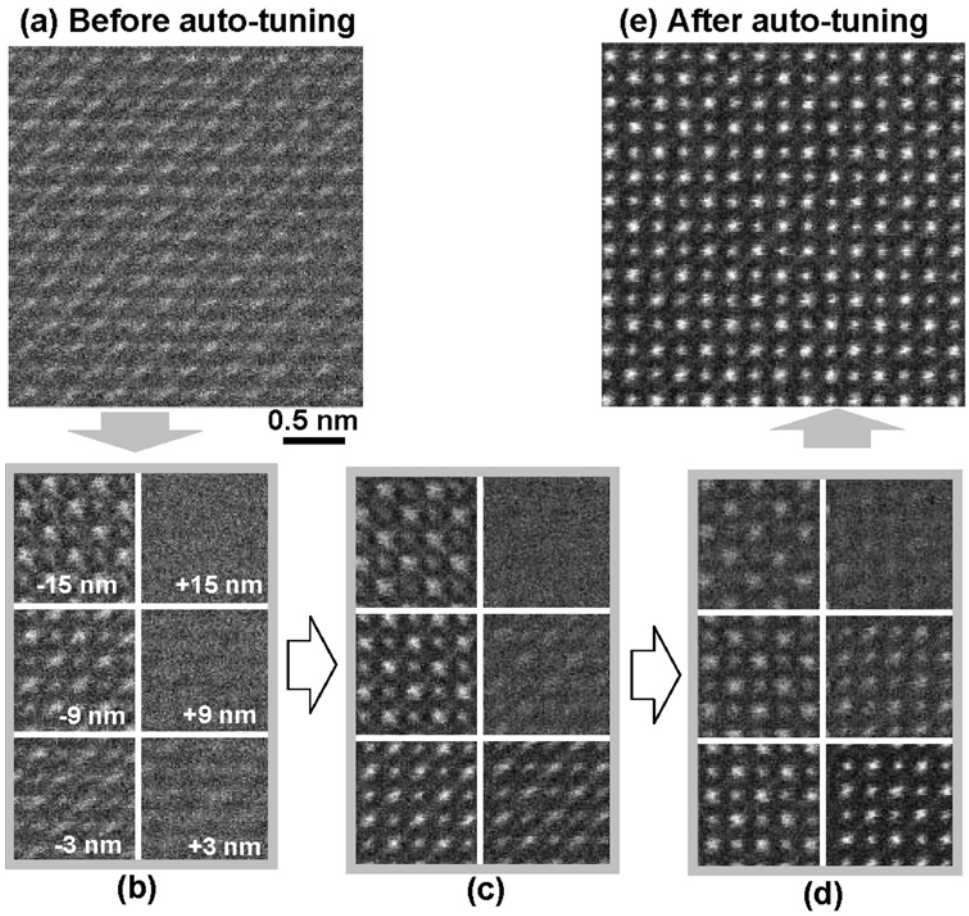

Figure 4. High-resolution HAADF-STEM images of [100]-projected $SrTiO_3$ (**a**) before and (**e**) after five iterations of the SIAM process. (**b**) First, (**c**) third, and (**d**) fifth sets of six focal-series images using the SIAM measurement procedure. The six focal series with 64 × 64 pixels were obtained by changing the defocus interval of 6 nm and using a scan speed of 20 μs/pixel.

Figure 3d, indicating that two defocused images (Figs. 3a, 3b) were actually taken across the Gaussian focus position. First-order aberrations were determined in the pair of images: the defocus value of 2.52 nm and the twofold astigmatism of 9.12 nm with a stigmation angle of −43.29°.

In comparison to the previous example shown in Figure 2, the twofold astigmatism is increased only by ~7 nm. However, this relatively small deviation in the twofold astigmatism appears significantly in both HAADF-STEM images and autocorrelation patterns. As mentioned above, even a fine drift in the first-order aberrations that occurs any time after the original aberration tuning with the standard specimen may catastrophically destroy the atomic resolution conditions. Therefore, it is very useful to measure the aberration status on actual crystallographic specimens. A procedure of *ad hoc* aberration tuning by the SIAM method is described in the following section.

Experimental Demonstration of Auto-Tuning by the SIAM Method

Figure 4 shows high-resolution HAADF-STEM images of [100]-projected $SrTiO_3$ (a) before and (e) after auto-tuning processing by the SIAM method. Since the focus and twofold astigmatism values were largely deviated from the optimum point, the atomic columns are barely visible, as shown in Figure 4a. In this auto-tuning process via the SIAM method, five iteration steps were performed, where the total time of the procedure was 68 s in this test (about 14 s per one set). At each iteration step, a set of six focal-series HAADF-STEM images taken at defocus values of −15, −9, −3, 3, 9, and 15 nm from the original focal point was acquired for aberration measurement by the SIAM method. Based on the defocus and twofold astigmatism values determined after each iteration step, appropriate shift values of the objective lens excitation and stigmators to compensate the measured aberrations were fed into the instrument automatically through a script in the Gatan DigitalMicrograph platform (Gatan, Inc., Pleasanton, CA). Figures 4b–4d show sets of focal series image at the first, third, and fifth (final) iteration, respectively. After each individual SIAM steps, distinct progress can be seen in the auto-tuning procedure. In addition to Gatan DigitalMicrograph, the SIAM method will be available in the JEOL-based TEM operation software as well. The reduction in the residual aberrations of defocus and twofold astigmatism after each SIAM step is shown in Figures 5a and 5b, respec-

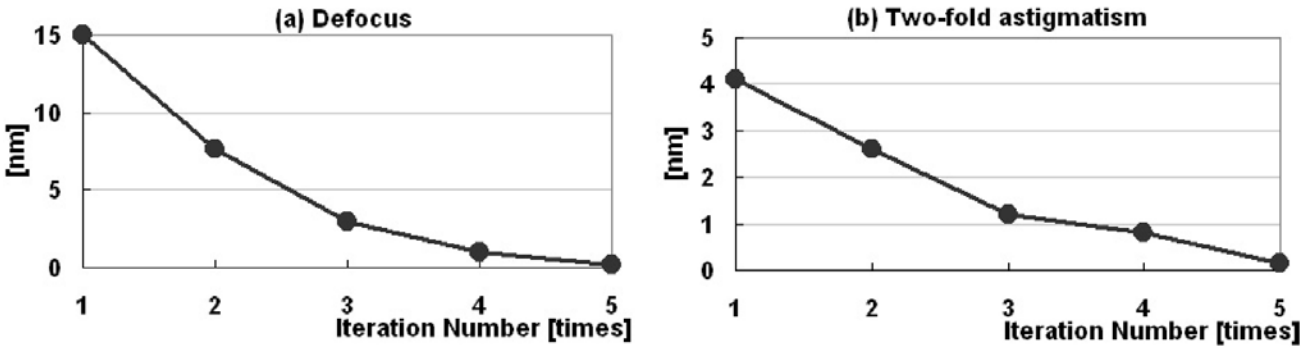

Figure 5. Progress of aberration measurement at each SIAM iteration step: (**a**) defocus and (**b**) twofold astigmatism.

tively. Both of the residual aberrations were gradually reduced through the iterative SIAM procedure of aberration measurement and compensation feedback to the microscope. By applying the SIAM auto-tuning method, the atomic-resolution STEM image appeared clearly without any manual adjustment, as shown in Figure 4e.

Summary

To tune first-order geometrical aberrations automatically before acquiring STEM images, a method for measuring aberrations in the probe-forming lens system using high-resolution STEM images from an oriented crystalline specimen (SIAM) was developed. In this method, the autocorrelation functions obtained from segmented areas of high-resolution STEM images are applied to determine the values of defocus and twofold astigmatism. The autocorrelation functions from a HAADF-STEM image are fitted with an elliptic function to estimate the probe-shape function with residual aberrations. By taking a set of autocorrelation functions from several segmented regions in a set of focal series HAADF-STEM images, the values of the defocus and twofold astigmatism are determined with the calibrated focal step of the objective lens. In this study, the *ad hoc* auto-tuning procedure for the defocus and twofold astigmatism was successfully demonstrated by applying the SIAM method without manual adjustment. The SIAM auto-fine-tuning procedure assists users with any experience in obtaining atomic-resolution images using aberration-corrected STEM.

Acknowledgments

The author (M.W.) wishes to acknowledge financial support from the National Science Foundation through grants DMR-0804528 and DMR-1040229.

References

Cowley, J.M. (1986). Electron diffraction phenomena observed with a high resolution STEM instrument. *J Electron Micr Tech* **3**, 25–44.

Dellby, N., Krivanek, O.L., Nellist, P.D., Batson, P.E. & Lupini, A.R. (2001). Progress in aberration-corrected scanning transmission electron microscopy. *J Electron Microsc* **50**, 177–185.

Haider, M., Uhlemann, S., Schwan, E., Rose, H., Kabius, B. & Urban, K. (1998). Electron microscopy image enhanced. *Nature* **392**, 768–769.

Haider, M., Uhlemann, S. & Zach, J. (2000). Upper limits for the residual aberration of a high-resolution aberration-corrected STEM. *Ultramicroscopy* **81**, 163–175.

Hosokawa, F., Sannomiya, T., Sawada, H., Kaneyama, T., Kondo, Y., Hori, M., Yuasa, S., Kawazoe, M., Nakamichi, Y., Tanishiro, T., Yamamoto, N. & Takayanagi, K. (2006). Design and development of Cs correctors for 300kV TEM and STEM. *IMC* **16**, 582.

Krivanek, O.L., Dellby, N. & Lupini, A.R. (1999). Towards sub-Å electron beams. *Ultramicroscopy* **78**, 1–11.

Lin, J.A. & Cowley, J.M. (1986). Calibration of the operating parameters for an HB5 STEM instrument. *Ultramicroscopy* **19**, 31–42.

Lupini, A.R., Wang, P., Nellist, P.D., Kirkland, AI. & Pennycook, S.J. (2010). Aberration measurement using the Ronchigram contrast transfer function. *Ultramicroscopy* **110**, 891–898.

Ramasse, Q.M. & Bleloch, A.L. (2005). Diagnosis of aberrations from crystalline samples in scanning transmission electron microscopy. *Ultramicroscopy* **106**, 37–56.

Rose, H. (1990). Outline of a spherically corrected semiaplanatic medium-voltage transmission electron microscope. *Optik* **85**, 19–24.

Rudnaya, M.E., Broek, W. Van den, Doornbos, R.M.P., Mattheij, R.M.M. & Maubach, J.M.L. (2011). Defocus and twofold astigmatism correction in HAADF-STEM. *Ultramicroscopy* **111**, 1043–1054.

Sawada, H., Sannomiya, T., Hosokawa, F., Nakamichi, T., Kaneyama, T., Tomita, T., Kondo, Y., Tanaka, T., Oshima, Y., Tanishiro, Y. & Takayanagi, K. (2008). Measurement method of aberration from Ronchigram by autocorrelation function. *Ultramicroscopy* **108,** 1467–1475.

Sawada, H., Sasaki, T., Hosokawa, F., Yuasa, S., Terao, M., Kawazoe, M., Nakamichi, T., Kaneyama, T., Kondo, Y., Kimoto, K. & Suenaga, K. (2009). Correction of higher order geometrical aberration by triple three-fold astigmatism field. *J Electron Microsc* **58**, 341–357.

Sawada, H., Watanabe, M., Okunishi, E. & Kondo, Y. (2011). Auto-tuning of aberrations using high-resolution STEM images by auto-correlation function. *Microsc Microanal* **17**(S2), 1308–1309.

Yamazaki, T., Kotaka, Y., Kikuchi, Y. & Watanabe, K. (2006). Precise measurement of third-order spherical aberration using low-order zone-axis Ronchigrams. *Ultramicroscopy* **106**, 153–163.